



Green Synthesized Unmodified Silver Nanoparticles as Reproducible Dual Sensor for Mercuric Ions and Catalyst to Abate Environmental Pollutants

Mamatha Susan Punnoose¹ · D. Bijimol¹ · Thomas Abraham¹ · Neena John Plathanam¹ · Beena Mathew¹

Accepted: 14 June 2021 / Published online: 26 June 2021

© The Author(s), under exclusive licence to Springer Science+Business Media, LLC, part of Springer Nature 2021

Abstract

The present study involves the green synthesis of unmodified silver nanoparticles using the aqueous leaf extract of *Mimosa diplotricha* (AgNP-MD). This work highlights the reliable optical and electrochemical sensing of Hg²⁺ ion (5–45 μM) by AgNP-MD with high selectivity. Optical sensing was easily identified by the color change of AgNP-MD to colorless upon effective interaction of metal nanoparticles with mercuric ions, which is in accordance with the decrement in surface plasmon resonance (SPR) of nanoparticles. Electrochemical voltammetric sensing was performed using a platinum electrode modified with AgNP-MD (AgNP-MD-Pt). The limit of detection (LOD) of the developed green sensor for mercuric ions was calculated from differential pulse voltammetry (DPV) analysis as 1.46 μM. The applicability of unmodified AgNP-MD towards Hg²⁺ ions was inspected for the collected real water samples. Ultraviolet–visible (UV–vis) spectrophotometer, Fourier transform infrared (FT-IR), X-ray diffraction (XRD), transmission electron microscopy (TEM), zeta potential, and dynamic light scattering (DLS) techniques were used to characterize the synthesized AgNP-MD and AgNP-MD-Hg²⁺ complexation. Moreover, the catalytic potential of green synthesized AgNP-MD towards the reduction of methyl orange and methylene blue was also evaluated. Both the degradations were fast, completed within few minutes, and followed pseudo-first-order kinetics with good regression coefficients. To the best of our knowledge, this is the first report on the synthesis of AgNP-MD using MD extract and its multifunctional applications including the fields of sensors and catalysis.

Keywords Silver nanoparticles · *Mimosa diplotricha* · Biosynthesis · Mercury ion · Sensing · Optical · Electrochemical · Nanocatalyst · Reduction · Organic dyes

1 Introduction

The acquisition of toxic heavy metals drastically affects the availability of fresh water and is often categorized as environmental teratogens. Mercury is the second toxic heavy metal which causes several health threats even to the developing fetus [1]. Its high affinity for thiol groups in proteins and enzymes leads to severe damages in the brain, kidney, lungs, and central nervous system [2]. Usually, mercury poisoning occurs from ingestion, inhalation, dermal absorptions, and dental amalgams. Due to its accumulative nature, it easily gets into the food chain, through marine fishes which absorb methyl mercury, the most toxic organic form of mercury [3].

Volcanoes and erosion of mineral deposits are the natural sources of mercury pollution. Human activities such as metal smelting, combustion of fossil fuels, chemical synthesis, and incineration of solid waste contribute large quantities of mercury to the environment [4]. According to the World Health Organization (WHO), mercury in drinking water is limited to 30 nM [5]. The anomalous concentration of Hg²⁺ ion leads to mercury poisoning which may finally lead to death. Therefore, a highly selective and sensitive technique is required for the detection of mercury ions.

Several reported methods for the monitoring of mercury ions involve cold vapor atomic fluorescence (CV-AFS) [6], inductively coupled plasma mass spectrometry (ICP-MS) [7], atomic absorption spectroscopy (AAS) [8], high-performance liquid chromatography (HPLC) [9], and flame photometry [10]. These methods include complex procedures, strenuous pre-treatment processes, and very expensive instrumentation. Few works on the sensing of mercury ions using biofunctionalized silver nanoparticles are reported [11–13].

✉ Beena Mathew
beenamscs@gmail.com

¹ School of Chemical Sciences, Mahatma Gandhi University, 686560, Kottayam, Kerala, India

An optical assay based on silver nanoparticles is an attractive method for the proper detection of Hg^{2+} ions due to its low cost, simplicity, and ease of measurement. The optical sensing in the presence of Hg^{2+} ions involves a remarkable color change of silver nanoparticles from yellowish-brown to colorless [14]. The yellowish-brown color of the silver nanoparticles is accredited to its optical properties and surface plasmon resonance (SPR). Heavy metal ions such as Hg^{2+} , Cd^{2+} , and Pb^{2+} can undergo electrochemical redox properties in an extremely fast way. Fast analysis, high specificity, and sensitivity of voltammetric technique make it convenient for the sensing of metal ions. So the green synthesized AgNP can be used for the reliable detection of Hg^{2+} ions in an aqueous solution. In contrast to other metal nanoparticles, the stability of silver nanoparticles for up to several months enables their utilization as a selective sensor for Hg^{2+} ions.

The recent progress in nanoscience and nanotechnology provided new platforms for the synthesis and applications of green metallic nanoparticles. Metal nanoparticles especially those of silver have a bunch of peculiar properties such as optical, thermal, electrical, and biological, which make them beneficial in sensing, medicine, catalysis, and water purification [15–18]. These applications are attributed to the unique size, morphology, and stability of silver nanoparticles [19, 20]. The different physical and chemical methodologies available for the synthesis of silver nanoparticles involve high cost, toxic chemicals, and drastic reaction conditions which often result in environmental toxicity and chemical hazards. Hence, biological means of silver nanoparticle synthesis particularly via plant extract is a virtuous green substitute for the traditional physicochemical methods. The recent research mainly focuses on the plant-mediated synthesis of silver nanoparticles due to its harmless nature, environmental friendliness, and cost-effectiveness. And the remarkable features of plant extract involving large natural availability, safety in handling, and its ability to act as both reducing and stabilizing agents contributed to its precedence.

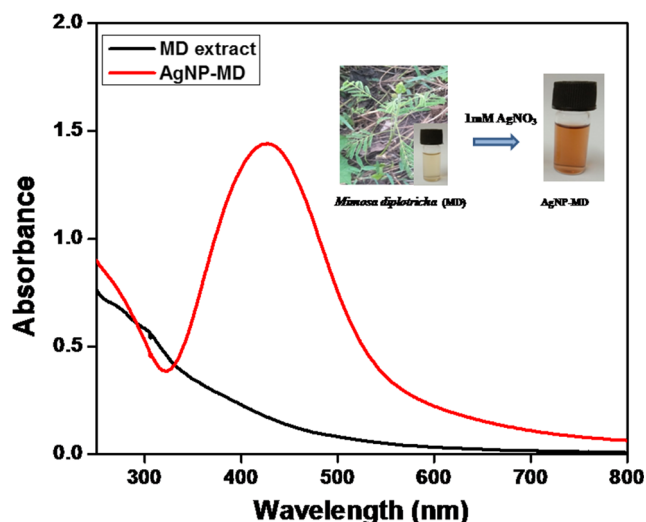


Fig. 1 Synthesis and formation of AgNP-MD

Though the green approach towards nanoparticle synthesis is highly favored, the time required for the completion of the reaction may vary from several hours to days. Irrespective of the conventional heating techniques, microwave irradiation provides fast and uniform heating which leads to the homogenous nucleation conditions for the formation of nanoparticles [21], and thus, the major flaw of large time consumption in biomediated method is efficiently overcome. Numerous reports on plant extract-mediated biosynthesis of silver nanoparticles by utilizing microwave energy are available. Moreover, the microwave technique is a rather easy, facile, rapid, and controlled method for the synthesis of nanoparticles [11, 13, 21].

Dye effluents from paint, plastic, paper, printing, textiles, drugs, leather, and food-related industries are the major organic pollutants in water [22, 23]. More than 7×10^5 tons of approximately 1,00,000 types of dyes are produced annually [24]. In addition to the toxic and carcinogenic effects, discharge of dye contaminants into the aquatic systems causes eutrophication and reduces sunlight penetration and dissolved oxygen content which interfere with the growth of aquatic species [25, 26]. Dyes are not readily biodegradable as they resist microbial attack and aerobic digestion. Because of the high chemical stability and inertness towards heat, light, and oxidizing agents, dyes are not susceptible to annihilation by conventional methods such as adsorption, ultrafiltration, photochemical, and electrochemical methods [27]. The highly persisting nature of organic contaminants even at their very low concentrations makes the water more detrimental for use. Recently, silver nanoparticles have emerged as an effective catalyst for the degradation of dye pollutants. The unique size, large surface-to-volume ratio, and electronic properties of nanoparticles which are absent in their bulk counterparts mainly contribute to its improved catalytic efficiency [28, 29].

In this work, a microwave-assisted approach was used for the synthesis of silver nanoparticles using an aqueous leaf extract of *Mimosa diplotricha* (MD). *Mimosa diplotricha* belongs to the family *Fabaceae* and is commonly known as a giant sensitive plant. They also hold antimalarial, antiviral, antibacterial, and antiparasitic properties. The phytochemical screening reveals that the leaves contain alkaloids, carbohydrates, saponins, glycosides, flavanoids, phenols, and tannins [30, 31]. These phytochemicals not only reduce the Ag^{1+} to Ag^0 via π electron transfer but also provide stability and prevent the nanoparticles from agglomeration.

The present study involves an unmodified microwave-assisted green synthesis of silver nanoparticles (AgNP-MD) using *Mimosa diplotricha* (MD) plant extract as both the reducing and stabilizing agent for the first time. Effect on various reaction parameters such as plant extract to silver nitrate ratio, microwave reaction time, and power of microwave radiation on the synthesis of AgNP-MD was explored. The AgNP-MD synthesis under the optimal conditions was characterized by ultraviolet–visible (UV–vis) spectrophotometer, FT-IR, DLS, zeta potential, XRD, and TEM analysis. The

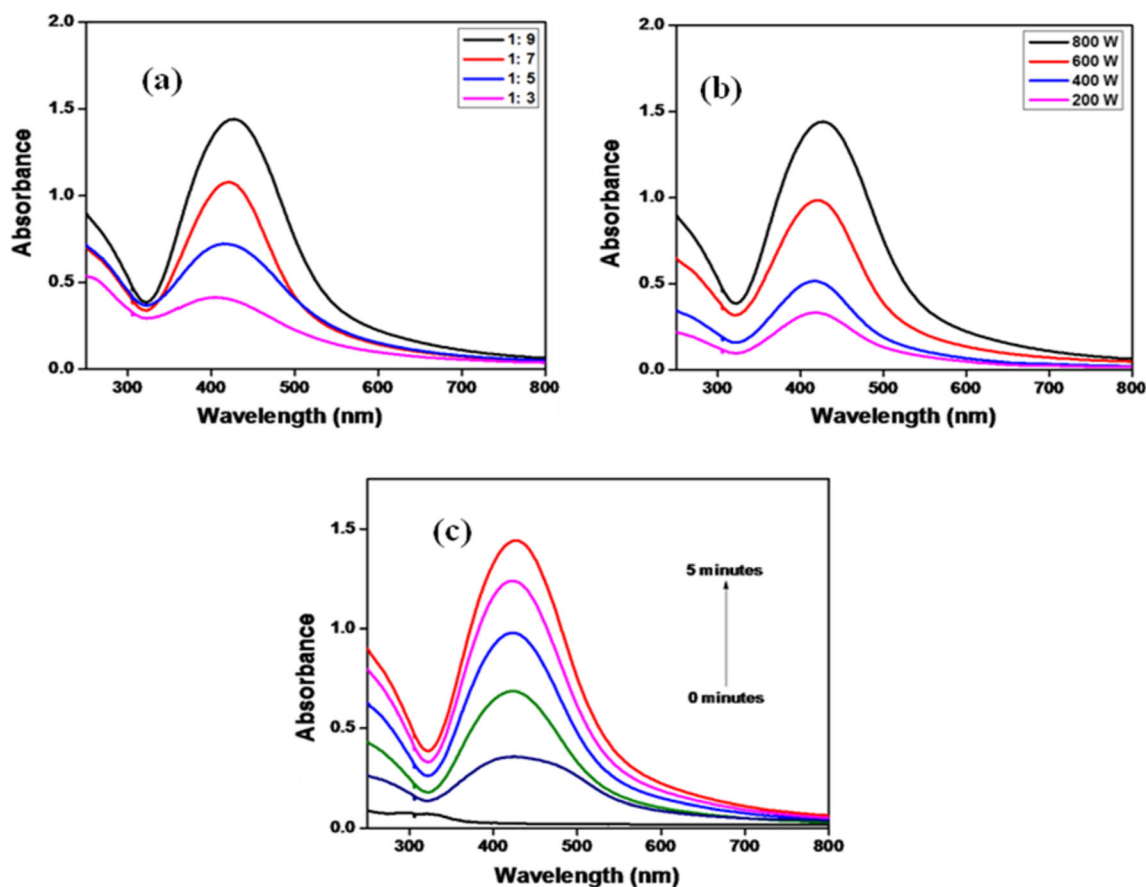


Fig. 2 Dependence of **a** composition of AgNO₃ and MD extract, **b** microwave power level, and **c** time on the formation of AgNP-MD

reliable selective sensing of AgNP-MD was displayed via optical and electrochemical methods for the detection of highly toxic Hg²⁺ ions at micromolar concentration. The applicability of the developed AgNP-MD green sensor was checked for real water samples collected. The catalytic activities of AgNP-MD were examined for the degradation of organic dyes, namely, methyl orange and methylene blue.

2 Experimental

2.1 Materials

Mimosa diplotricha leaves were collected from Njeezhoor, Kerala, India. Silver nitrate (AgNO₃), sodium borohydride (NaBH₄), methyl orange, methylene blue, and

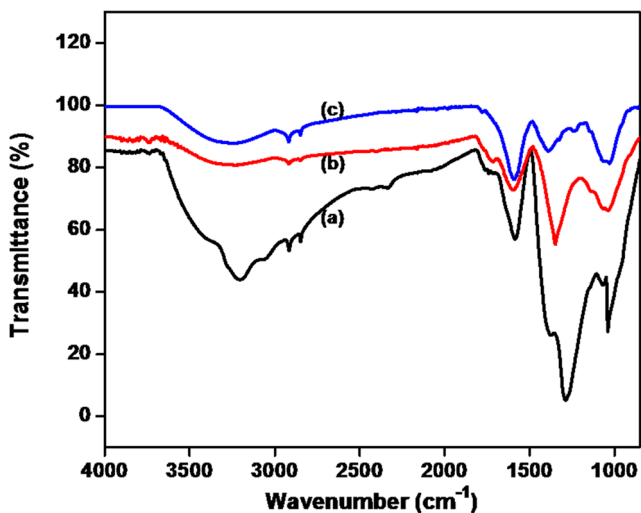


Fig. 3 FT-IR spectra of **a** *Mimosa diplotricha* extract, **b** AgNP-MD, and **c** AgNP-MD-Hg²⁺ complex

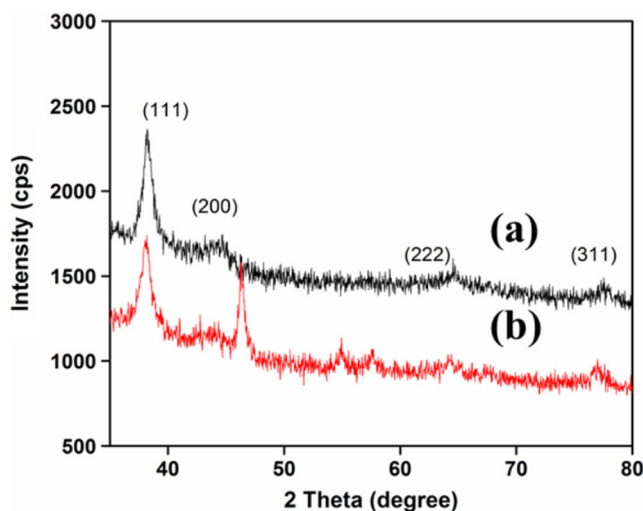


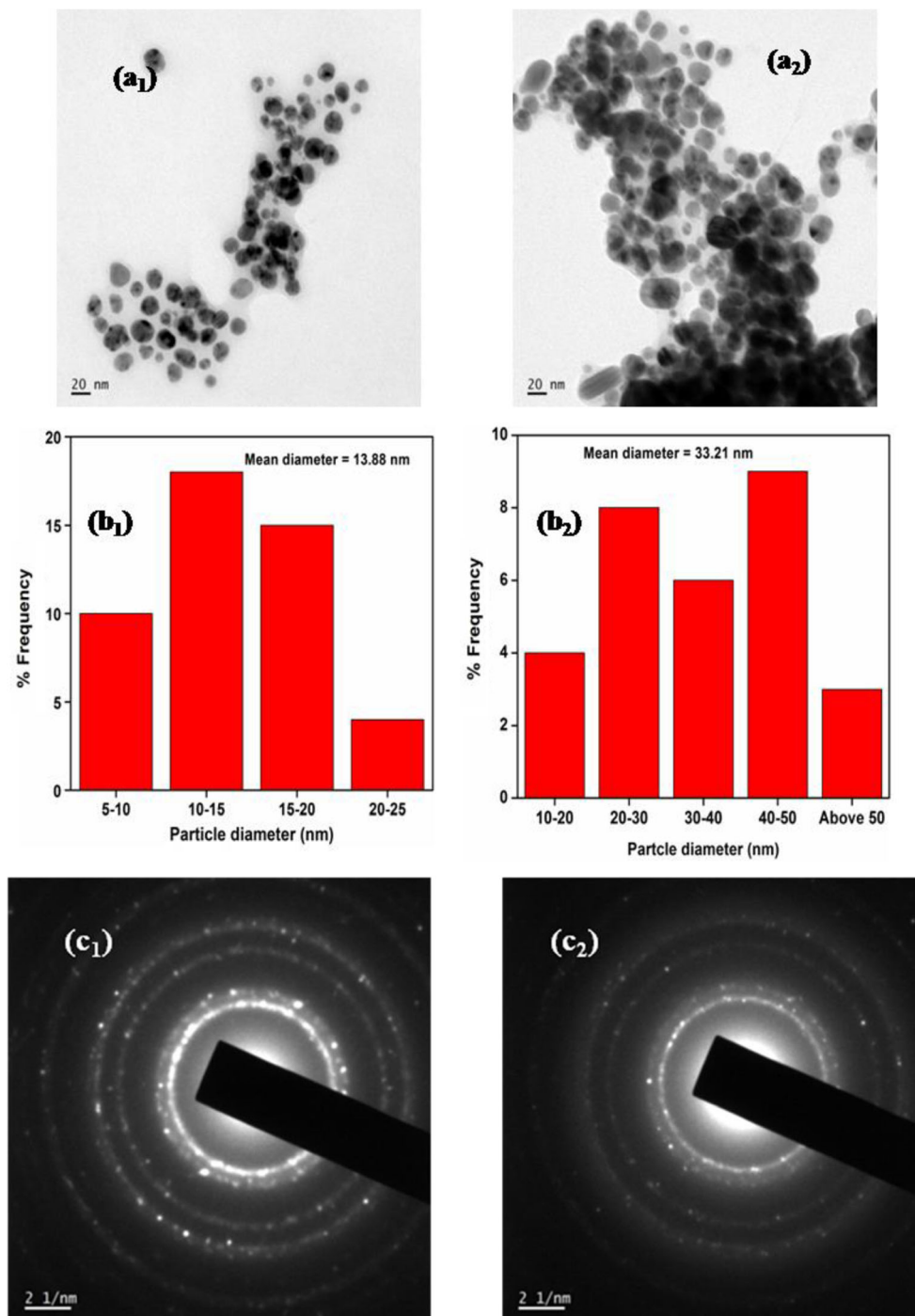
Fig. 4 XRD pattern of **a** AgNP-MD and **b** AgNP-MD-Hg²⁺ complex

metal chlorides, namely, mercuric chloride (HgCl_2), copper chloride (CuCl_2), manganese chloride (MnCl_2), nickel chloride (NiCl_2), cobalt chloride (CoCl_2), zinc chloride (ZnCl_2), lead chloride (PbCl_2), and cadmium chloride (CdCl_2) of analytical grade, were purchased from Merck (India). All chemicals were used without any further purification. Double distilled (DD) water was used throughout the experiment.

2.2 Instruments

The UV–vis absorption spectra were recorded using Shimadzu UV-2450 spectrometer (Japan). FT-IR studies were done using the Perkin Elmer-400 FT-IR spectrometer (Singapore) at a frequency range of $400\text{--}4000\text{ cm}^{-1}$. X-ray diffraction studies of synthesized AgNP-MD were conducted on Bruker AXS D8 Advance X-ray Diffractometer (USA).

Fig. 5 TEM images of **a₁** AgNP-MD and **a₂** AgNP-MD- Hg^{2+} ; particle size histogram of **b₁** AgNP-MD and **b₂** AgNP-MD- Hg^{2+} ; and SAED patterns of **c₁** AgNP-MD and **c₂** AgNP-MD- Hg^{2+}



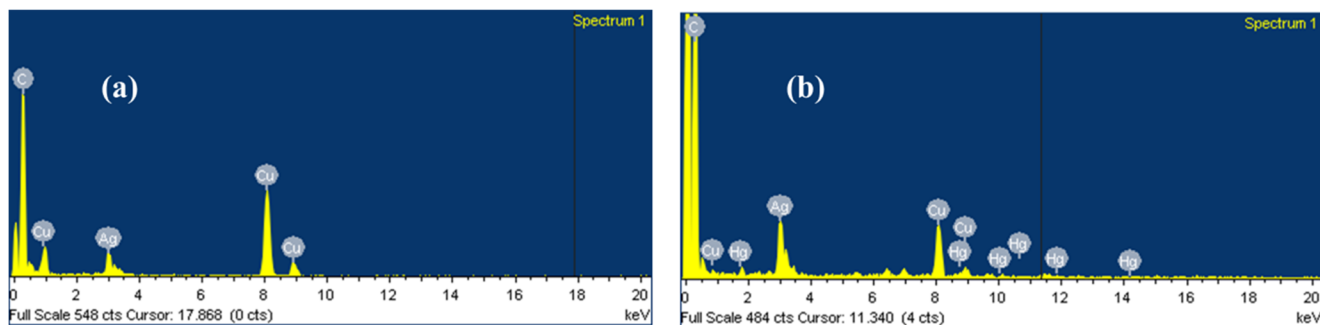


Fig. 6 EDX spectra of **a** AgNP-MD and **b** AgNP-MD-Hg²⁺ complex

Transmission electron microscopic and energy dispersive X-ray images were obtained from the JOEL JEM-2100 model microscope (Japan). The particle size analysis and zeta potential measurements were done using Horiba SZ-100 scientific nanoparticle analyzer (Japan). Electrochemical studies were performed on Biologic SP-300 electrochemical workstation (Germany) using Pt electrode modified by AgNP-MD as the working electrode. The Ag/AgCl and Pt wire electrode were used as the reference and counter electrodes, respectively.

2.3 Preparation of *Mimosa diplotricha* Extract

About 25 g of the fresh green leaves of *Mimosa diplotricha* was washed thoroughly and boiled for 1 h in 100 ml distilled water. The solution was cooled, filtered, and stored at 4°C for further use.

2.4 Synthesis of Silver Nanoparticles Using *Mimosa diplotricha* Extract (AgNP-MD)

For the microwave-assisted synthesis, the freshly prepared plant extract was thoroughly mixed with a 1-mM solution of AgNO₃ in a 1:9 ratio. The solution was subjected to irradiation for 5 min in a domestic microwave oven (Sharp R-219T(W)) operating at a power of 800 W and frequency of about 2450 MHz.

The formation of silver nanoparticles was monitored using a UV–vis spectrophotometer. The yellowish-brown coloration of the solution indicated the formation of AgNP-MD.

2.5 DLS and Zeta Potential Measurements

The synthesized yellowish-brown solution of AgNP-MD was mixed with 45 μM HgCl₂ in an appropriate ratio and was sonicated. The color of the colloidal solution changed to colorless. The AgNP-MD and AgNP-MD mixed with Hg²⁺ solutions were separately analyzed at 25°C using the particle size analyzer, and the obtained hydrodynamic diameters were the result of light scattering by the particles suspended within the solution. The zeta potentials of these solutions were also measured.

2.6 Optical Sensing of Hg²⁺ Ions by AgNP-MD

For the optical sensing of the metal ions, the definite volume of the AgNP-MD solution was shaken with known concentration of various concentrations of Hg²⁺ ions ranging from 5 to 45 μM, which involves a remarkable visual color change of AgNP-MD from yellowish-brown to colorless. The analyses were done using a UV–vis spectrophotometer.

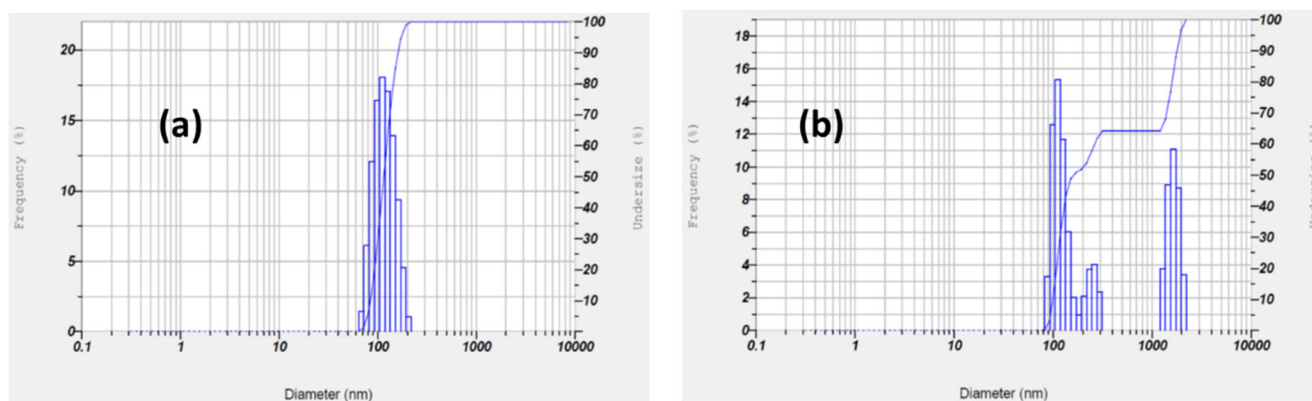


Fig. 7 Particle size distribution of **a** AgNP-MD and **b** AgNP-MD-Hg²⁺ by DLS analysis

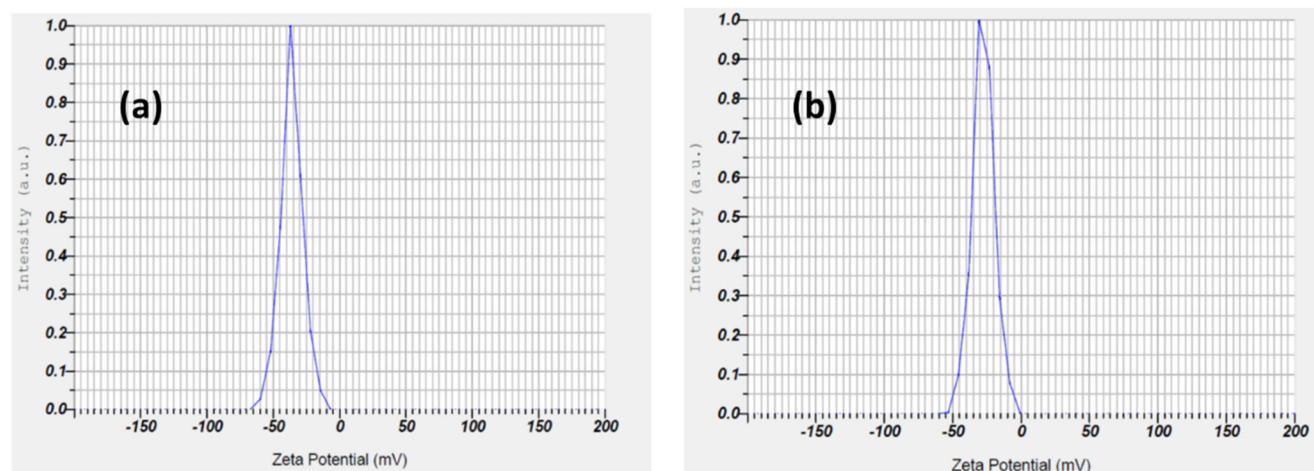


Fig. 8 Zeta potentials measurements of **a** AgNP-MD and **b** AgNP-MD-Hg²⁺

2.7 Optical Selectivity of AgNP-MD Towards Hg²⁺ Ions

In order to examine the selectivity of AgNP-MD towards Hg²⁺ ions among the various divalent metal ions, a fixed amount of AgNP-MD solution was mixed separately with each of the metal ion solutions of equal concentration. Each of the solution mixtures was then analyzed using a UV–vis spectrophotometer.

2.8 Fabrication of AgNP-MD Modified Platinum Electrode

The surface of the bare Pt electrode was cleaned with a polishing alumina slurry (10 μM) to a mirror finish. It was washed several times with DD water, in order to ensure the cleanliness of the electrode surface. About 5 μL of AgNP-MD was allowed to dry on the surface of the Pt electrode. For all the electrochemical experiments, AgNP-MD modified platinum (AgNP-MD-Pt) electrode was used as the working electrode.

2.9 Electrochemical Sensing of Hg²⁺ Ions by AgNP-MD-Pt

The electrochemical studies were carried out using cyclic voltammetry (CV) and differential pulse voltammetry (DPV) techniques. The cyclic voltammetric studies were carried out in 0.1 M acetate buffer solution (ABS) of pH 6 at a potential range from −0.2 to 0.5 V. The effects of scan rate and concentration of Hg²⁺ ions on the sensing by AgNP-MD-Pt were studied using the CV technique. Differential pulse voltammetry (DPV) studies were carried out in ABS with successive addition of various concentrations of Hg²⁺ ions at a pulse amplitude of 25 mV and pulse width of 200 ms. The limit of detection of Hg²⁺ ion was found using DPV analysis. Both CV and DPV studies were carried out at 25°C.

2.10 Electrochemical Selectivity of AgNP-MD Towards Hg²⁺ ions

The cyclic voltammetric selectivity involves the electrochemical behavior of AgNP-MD-Pt in the presence of each of the various divalent metal ion solutions of the same concentration. The selectivity studies were carried out in ABS (0.1 M, pH = 6) at a fixed scan rate of 100 mVs^{−1}.

2.11 Preparation of Real Water Samples for Analysis

Tap water from Mahatma Gandhi University, Kottayam, Kerala, and river water from Njeezhoor, Kottayam, Kerala, were collected and used for the analysis. The collected water samples were centrifuged and filtered through a 0.22-μm membrane. The filtered samples were spiked with an appropriate amount of Hg²⁺ ions and were used for sensing of Hg²⁺ ions.

2.12 Catalytic Degradation of Organic Dyes

The catalytic activity of the synthesized AgNP-MD was investigated towards the degradation of dyes, methyl orange (1 × 10^{−4} M), and methylene blue (8 × 10^{−5} M). The procedure involved the mixing of 2.5 mL of the dye, 0.5 mL of NaBH₄ (0.06 M), and 0.25 mL AgNP-MD solution in a quartz cuvette of path length 1 cm. The progress of the catalytic degradation

Table 1 DLS and zeta potential values of AgNP-MD and AgNP-MD-Hg²⁺

Sample	DLS values (nm)	Zeta potential (mV)
AgNP-MD	119.6	−36.1
AgNP-MD-Hg ²⁺	682.8	−27.6

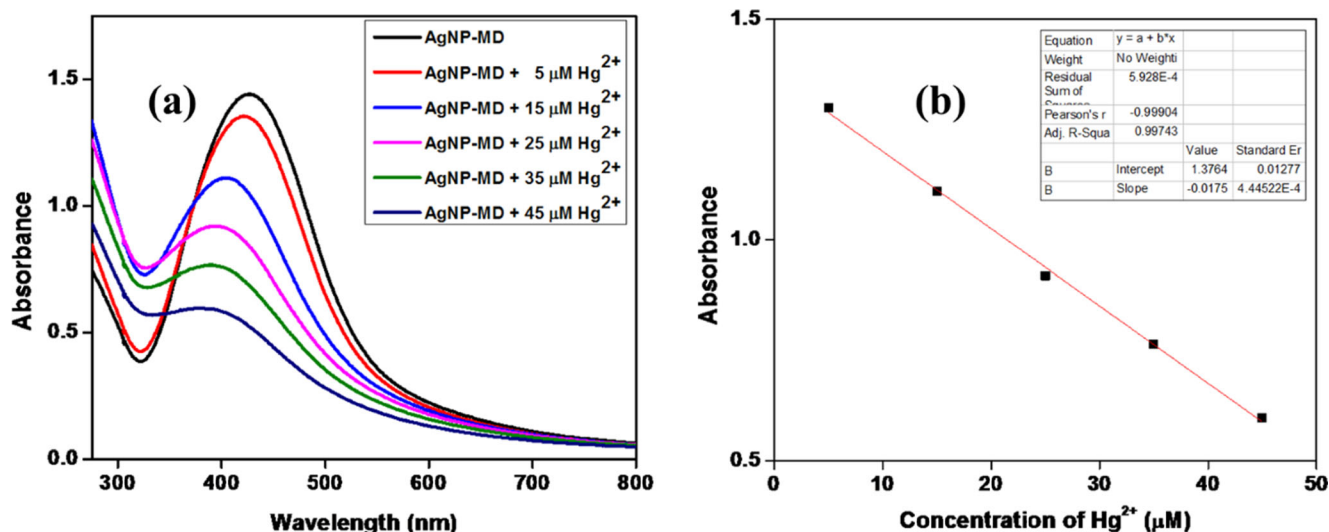


Fig. 9 **a** UV-vis spectra of AgNP-MD with various concentrations of Hg^{2+} ions and **b** linear plot of concentration of Hg^{2+} ions with absorbance

of the dyes was monitored using a UV-vis spectrophotometer at regular intervals of time.

3 Results and Discussion

3.1 Synthesis of AgNP-MD

The AgNP-MD formation was followed spectrophotometrically in the range 200–800 nm. The pale yellow color of the mixture of silver nitrate solution and *Mimosa diplotricha* extract changed to yellowish brown upon 5 min of microwave irradiation. This indicates the formation of AgNP-MD (Fig. 1) and is confirmed by a surface plasmon resonance (SPR) peak at 420 nm.

The synthesis of AgNP-MD was optimized by varying the composition, microwave power level, and irradiation time. For the synthesis of silver nanoparticles, different compositions of plant extract and silver nitrate were used for the experiment. Out of the different compositions studied, the 1:9 ratio was found to be optimum with the most intense and smooth peak as shown in Fig. 2a.

In order to study the influence of microwave power level on the formation of silver nanoparticles, the power of irradiation was varied between 200 to 800 W. Figure 2b clearly indicates that the intensity of the absorption peak increased and reached a maximum at a power of 800 W. The influence of irradiation time was also studied by monitoring the peak formation in 1:9 composition at every 1 min of irradiation at a power of 800 W. At a lower reaction time, AgNP-MD formation was not complete. After irradiation for 2 min, a sharp peak was observed at 420 nm. The intensity of this peak increased with irradiation time without much change in its position. No change in intensity was observed after 5 min of microwave irradiation which confirms the complete reduction

of Ag^+ to Ag^0 (Fig. 2c). The synthesized AgNP-MD was found stable up to 6 months when stored at 4°C , as their absorbance spectrum shows no observable alterations in comparison with the freshly prepared AgNP-MD (Fig. S1 of Supplementary material (SM)). This proves the capping and stabilization of AgNP-MD by the various phytochemicals present in the plant extract.

3.2 Characterization of AgNP-MD

3.2.1 FT-IR

Fourier transform infrared analysis was done to identify the presence of different functional groups present in MD, AgNP-MD, and AgNP-MD- Hg^{2+} complex (Fig. 3). The AgNP-MD shows prominent bands at 3230, 2923, 1584, 1390, and 1039 cm^{-1} which correspond to O–H stretching vibrations of

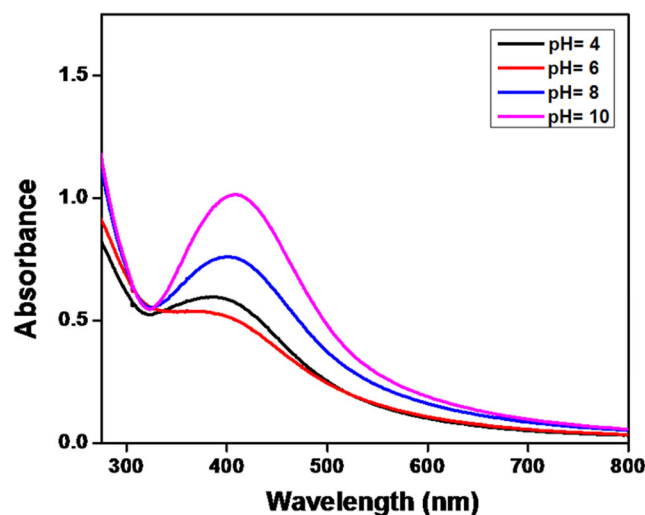
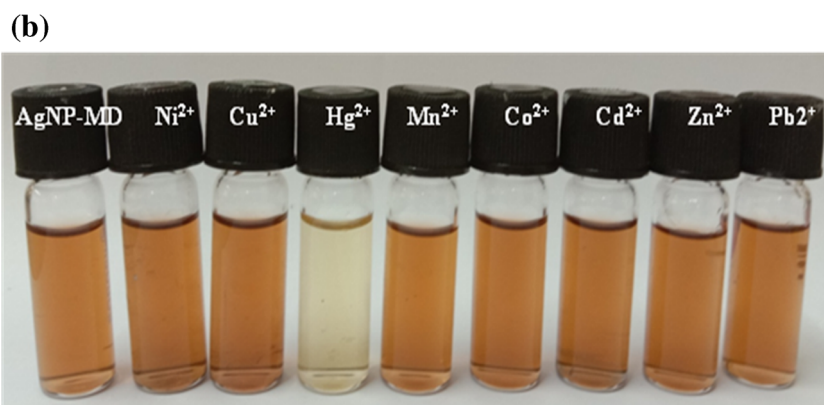
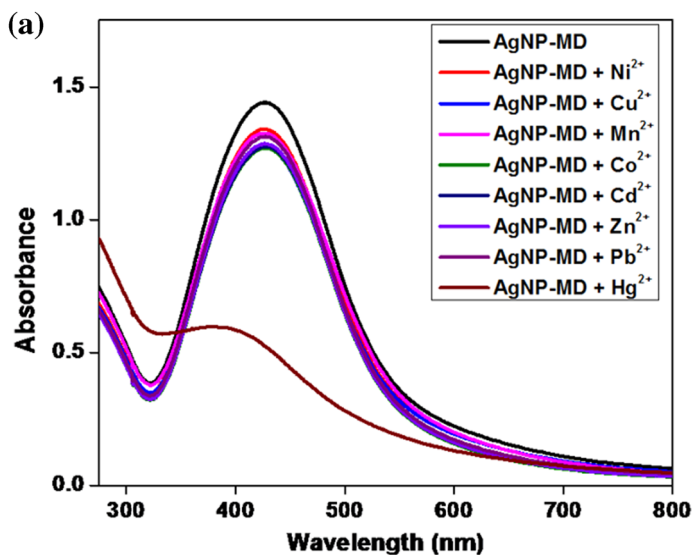


Fig. 10 UV-vis spectra of AgNP-MD with $45\text{ }\mu\text{M Hg}^{2+}$ ions at different pH

Fig. 11 **a** Selectivity study of AgNP-MD towards different metal ions. **b** Digital response of different metal ions towards the synthesized AgNP-MD



hydroxyl group present in the flavonoids and polyphenols, stretching vibration of aliphatic C–H groups, C=O stretching of carbonyl group and O–H bending of carboxylic acid group, and stretching vibration of C–O–C group, respectively [32].

All these functional groups arise from the various phytochemicals present in the MD extract. AgNP-MD on interaction with Hg^{2+} ion shows a decrease in the intensity of vibrational bands along with a slight shift in its band position.

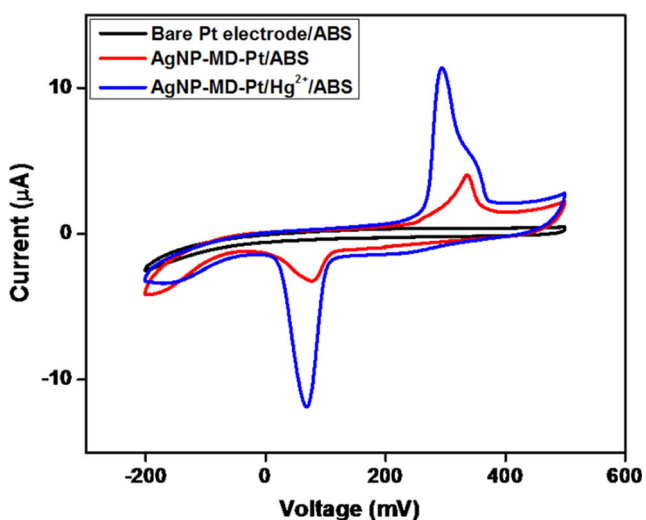


Fig. 12 Cyclic voltammogram of AgNP-MD-Pt electrode with a bare electrode

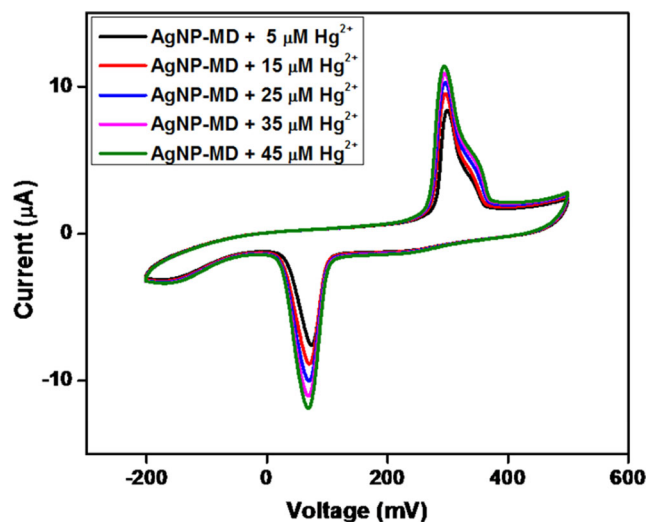


Fig. 13 Cyclic voltammogram of AgNP-MD-Pt electrode at different concentration of Hg^{2+} ion

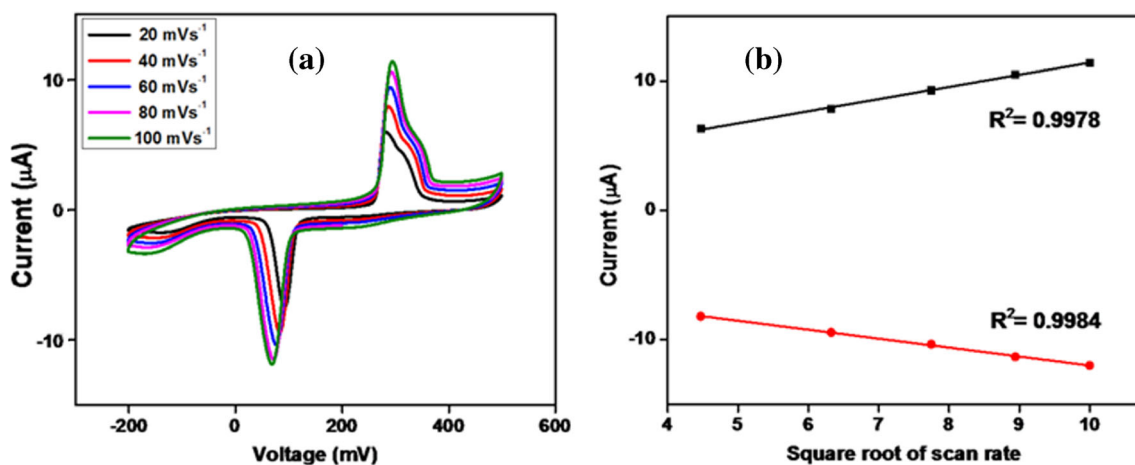


Fig. 14 **a** Effect of scan rate on the cyclic voltammetric response of AgNP-MD-Pt on 45 μM Hg^{2+} and **b** linear response of current versus square root of scan rate

3.2.2 XRD

The crystalline nature of the green synthesized AgNP-MD was confirmed by the XRD technique. Figure 4a shows four Bragg's diffraction peaks at 38.19° , 64.67° , 77.63° , and 81.61° which corresponds to the (111), (200), (220), and (311) facets of fcc lattice of AgNP-MD nanoparticles (JCPDS File 04-0783) [33, 34]. The additional peaks in Fig. 4b confirm the interaction of Hg^{2+} ions with AgNP-MD.

3.2.3 TEM Analysis

The morphology and distribution of the synthesized AgNP-MD and AgNP-MD complexed with Hg^{2+} were investigated using TEM analysis. Figure 5a₁ shows that most of the synthesized AgNP-MD are well dispersed spherical particles in the nano regime. The average particle size is found to be 13.88 nm from the histogram showing particle size distribution (Fig. 5b₁). The morphological changes and increase in particle size of AgNP-MD upon aggregation with Hg^{2+} ion were quite clear from Fig. 5a₂. The resultant increase in nanoparticle size to 33.21 nm is evident from Fig. 5b₂. Figure 5c₁ depicts bright spots in circular rings of selected area (electron) diffraction (SAED) pattern which confirmed the highly monodisperse crystalline nature of the synthesized AgNP-MD nanoparticles, while the faded spots of circular rings in Fig. 5c₂ revealed the low crystallinity of AgNP-MD due to its effective complexation with Hg^{2+} ions. These results are very similar to those of Cu^{2+} complexation with *Moringa oleifera* mediated silver nanoparticles (AgNP-MO) [20].

3.2.4 Energy Dispersive X-ray (EDX) Analysis

The elemental composition of AgNP-MD and AgNP-MD- Hg^{2+} are revealed by the EDX analysis. The energy dispersive X-ray (EDX) spectra of AgNP-MD are shown in Fig. 6a. The strong

signal at 3 Kev confirms the existence of AgNP-MD. The signals corresponding to the mercury confirms the complexation of Hg^{2+} ion with AgNP-MD in Fig. 6b. The copper signals are from the copper grid used for the sample preparation.

3.2.5 Particle Size Analysis and Zeta Potential Measurements

The presence of Hg^{2+} ion increased the particle size and decreased the zeta potential of AgNP-MD (Fig. 7 and Fig. 8). Results obtained from the DLS analysis and zeta potential measurements of AgNP-MD and AgNP-MD- Hg^{2+} are tabulated in Table 1. From the DLS measurements, the average particle size of AgNP-MD increased from 119.6 to 682.8 nm upon the addition of Hg^{2+} . And these particle diameters are found to be greater than their corresponding TEM results. This is due to fact that TEM provides the diameter of individual particles, while DLS determines the hydrodynamic diameter of the nanoparticles dispersed in the aqueous medium by

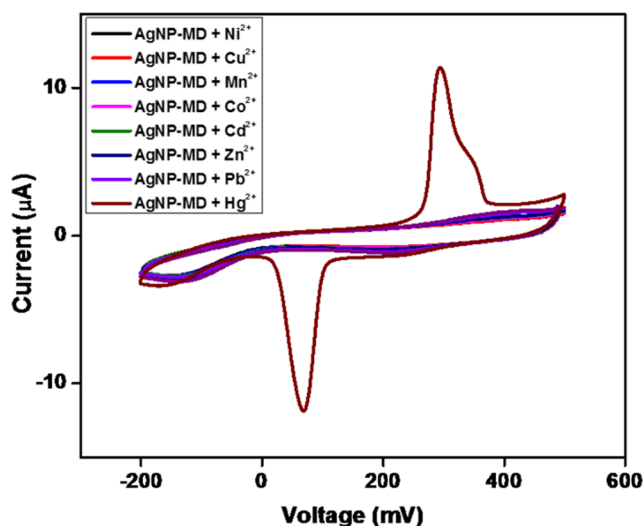


Fig. 15 Selectivity study of AgNP-MD-Pt electrode towards different divalent metal ions

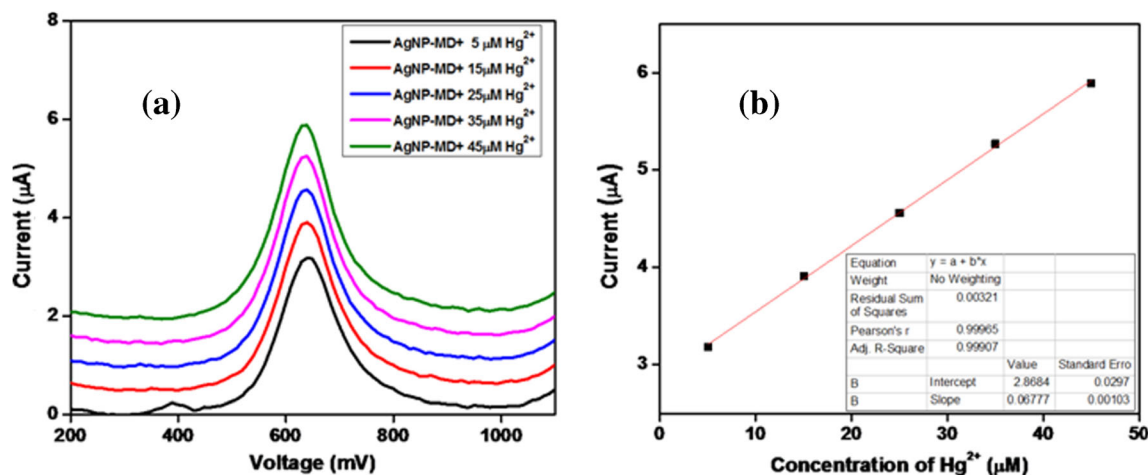


Fig. 16 a Differential pulse voltammetric response of AgNP-MD-Pt electrode towards various concentrations of Hg^{2+} and b linear plot of current versus various concentrations of Hg^{2+} ion

means of the light scattering from the nanoparticle core and surface layers covering the main core.

Zeta potential technique determines the surface charge of nanoparticles in an aqueous solution. Nanoparticles with zeta potential values more positive than +30 mV or more negative than -30 mV are assessed to be electrically stable [35]. The stability of AgNP-MD synthesized from plant extract is evident from the zeta potential measurement of -36.1 mV. On interaction with Hg^{2+} ions, the surface charge of AgNP-MD decreased to -27.6 mV which causes diminishment in the electrostatic bonding between the phytochemical constituents and AgNP-MD, leading to its destabilization and aggregation of the AgNP-MD.

3.3 Optical Sensing of Hg^{2+} Ions

3.3.1 Effect of Concentration of Hg^{2+} Ions

The synthesized unmodified AgNP-MD acts as an optical sensor for Hg^{2+} ions. In order to study the effect of Hg^{2+} ion concentration, successive additions of Hg^{2+} ions (5 to 45 μM) into AgNP-MD were carried out. The effectual interaction of AgNP-MD with Hg^{2+} ions resulted in the gradual lowering of the absorbance at 420 nm along with a slight blue shift in its SPR (Fig. 9). The yellowish-brown color of AgNP-MD changed to colorless upon successful surface interaction with Hg^{2+} ions.

A likely mechanism proposed for the optical sensing of Hg^{2+} ions on the surface of green synthesized silver nanoparticles involves a redox reaction between Hg^{2+} and Ag^0 . Upon the addition of Hg^{2+} ions, the capping agents on the surface of AgNP-MD move away, and the very slight electrochemical potential difference between the Hg^{2+} (0.85 V) and AgNPs (0.8 V) enables the easy oxidation of Ag^0 to Ag^{1+} which results in the fast reduction of Hg^{2+} to Hg^0 . The reduced Hg^0 forms an Hg-Ag nanoalloy on the nanoparticle surface which caused the discoloration of

the colloidal solution along with a gradual blue shift in the SPR band of AgNP-MD [36, 37]. In order to acquire stability, the destabilized amalgamated AgNP-MD undergoes aggregation to configure huge particle size and is evident from the TEM and DLS results. The formation of Ag-amalgam is clearly indicated by the decrease in surface charges of AgNP-MD particles as obtained from the zeta potential measurements. All the optical observations were monitored using a UV-vis spectrophotometer.

3.3.2 Effect of pH

The effect of pH on the optical sensing of Hg^{2+} ions by AgNP-MD is shown in Fig. 10. The silver nanoparticles in ABS of varying pH were prepared, and 45 μM Hg^{2+} ions were added into each of the solutions. The optical response of each of the solution mixture was noted using a UV-vis spectrometer. Maximum sensing of Hg^{2+} ions occurred at pH 6, and hence, it was selected as the optimum pH for further studies. At higher pH values, sensing was found to be minimum, and the solubility of AgNP-MD- Hg^{2+} decreases due to the precipitation of hydroxides.

Table 2 Comparison of present work with reported green synthesized sensors for Hg^{2+} ion

Method	Sensor	LOD (μM)	Reference
Optical	AgNP- <i>Soymida febrifuga</i>	13.32	[38]
	AgNP- <i>Carrageenan</i>	292.00	[39]
	AgNP- <i>Citrate/L-Cysteine</i>	3.00	[40]
	AgNP- <i>Mimosa diplotricha</i>	2.48	This work
Electrochemical	AgNP- <i>Arbutus andrachne</i>	8.43	[41]
	AgNP- <i>Agaricus Bisporus</i>	2.10	[11]
	AgNP- <i>Mimosa diplotricha</i>	1.46	This work

Table 3 Real water sample analysis of Hg²⁺ by AgNP-MD (*n* = 3)

Sample	Hg ²⁺ (μM)		Detection (%)	RSD (%)
	Added	Found		
Tap water	5	5.2 ± 0.05	104	1
	15	15.3 ± 0.09	102	0.6
River water	5	5.3 ± 0.09	106	1.8
	15	15.4 ± 0.12	102.6	0.8

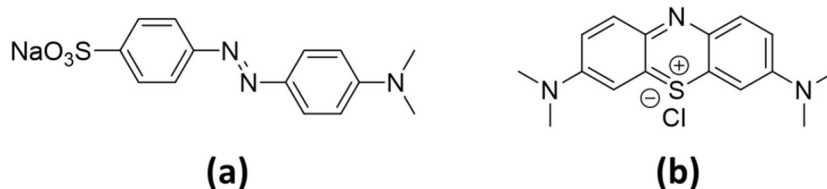
3.3.3 Selectivity of AgNP-MD Towards Hg²⁺ Ions

To study the selectivity of synthesized AgNP-MD towards various divalent metal ions, equimolar solutions (45 μM) of various metal ions such as Ni²⁺, Cu²⁺, Mn²⁺, Co²⁺, Cd²⁺, Zn²⁺, Pb²⁺, and Hg²⁺ were prepared and separately mixed with a definite volume of AgNP-MD solution (Fig. 11a). Upon mixing with Hg²⁺ ions, the yellowish-brown color of the AgNP-MD changed to colorless. No such prominent color change occurred for other metal ions though a slight decrease in the absorbance peak was observed. The lower reduction potential of transition, alkali, or alkaline earth metals restricts the oxidation of zero-valent AgNPs to Ag¹⁺, while the higher standard reduction potential of Hg²⁺ ion permits its facile selective sensing by AgNP-MD. The digital photographs of the color responses of AgNP-MD towards the various divalent metal ions are shown in Fig. 11b.

3.4 Electrochemical Sensing of Hg²⁺ Ion

The electrochemical sensing of AgNP-MD-Pt electrode towards Hg²⁺ ions was studied by voltammetric techniques such as cyclic voltammetry (CV) and differential pulse voltammetry (DPV). Figure 12 clearly depicts the electrochemical response of modified and unmodified electrodes in the cyclic voltammetric study. The bare Pt electrode exhibits no observable redox peaks in the cyclic voltammogram. AgNP-MD-Pt electrode shows a redox pair around 336 and 80 mV and is ascribed to Ag⁺/Ag conversion. The appearance of a high anodic peak current at about 293 mV and the cathodic peak current at 70 mV in the voltammogram confirms the reliable sensing of Hg²⁺ ions by AgNP-MD-Pt. The origin and variations of this redox couple indicate the effectual interaction of Hg²⁺ ions with AgNP-MD on the Pt electrode surface. Thus, AgNP-MD acts as a potent sensor for Hg²⁺ ions.

Fig. 17 Chemical structures of **a** methyl orange and **b** methylene blue



3.4.1 Effect of Concentration

In order to study the effect of concentration of Hg²⁺ ions on AgNP-MD-Pt electrode, cyclic voltammograms responses at different concentrations (5 to 45 μM) of Hg²⁺ in ABS at a fixed scan rate of 100 mVs⁻¹ were noted. Due to the large availability of electroactive species at higher concentrations, a progressive increase in redox peak current was observed with the increase in the concentration of Hg²⁺ ions (Fig. 13).

3.4.2 Effect of Scan Rate

The CV responses of AgNP-MD-Pt electrode towards Hg²⁺ ions at different scan rates were studied. Figure 14a clearly indicates that both the anodic and cathodic peak currents increased linearly with the scan rate. The redox peak showed a maximum response at a scan rate of 100 mVs⁻¹. A plot of redox peak current with the square root of scan rate shows a linear response (Fig. 14b).

3.4.3 Selectivity Study

The electrochemical responses of AgNP-MD-Pt electrode towards various divalent metal ions like Ni²⁺, Cu²⁺, Mn²⁺, Co²⁺, Cd²⁺, Zn²⁺, Pb²⁺, and Hg²⁺ ions were checked. The selectivity studies were carried out at a pH of 6 and with a scan rate of 100 mVs⁻¹. The electrochemical behavior of AgNP-MD-Pt electrode towards each of the metal solutions was noted separately. Figure 15 reveals that a redox couple response was only observed with Hg²⁺ ion and no such response was obtained in the presence of any other metal ions. The results pointed out the high selectivity of the developed green sensor towards the Hg²⁺. Thus, selective sensing of the fabricated AgNP-MD-Pt electrode towards Hg²⁺ ions makes it an efficient electrochemical sensor.

3.5 Differential Pulse Voltammetry (DPV)

DPV responses of AgNP-MD-Pt electrode towards different concentrations of Hg²⁺ between 5 to 45 μM were done (Fig. 16a). The peak current increased with the increase of Hg²⁺ concentration. A calibration curve plotted between current response against the concentration of Hg²⁺ ion gives a linear plot with a regression coefficient of 0.9990 (Fig. 16b). The limit of detection (LOD) value is calculated from the obtained data using the equation LOD = 3 s/m, where “m” is the slope

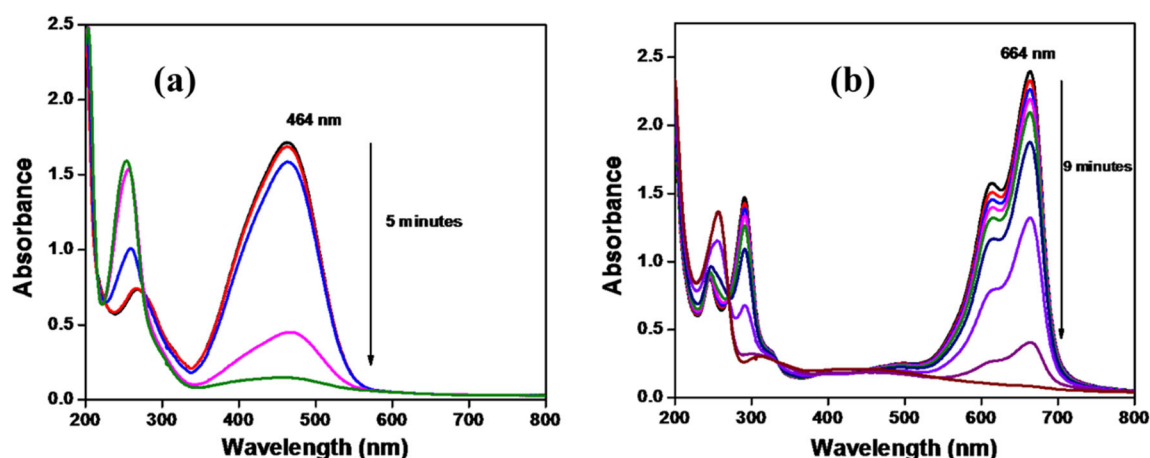


Fig. 18 UV–vis spectra of catalytic reduction reactions of **a** methyl orange and **b** methylene blue using 0.04 mg/mL AgNP-MD nanocatalyst

of the calibration curve and “s” represents the standard deviation of the linear responses. And thus LOD was estimated to be 1.46 μM . From Table 2, it is found that the AgNP-MD is an efficient sensor than other reported green synthesized sensors of Hg^{2+} .

3.6 Real Water Analysis

The efficiency of the developed sensor was tested for the analysis of real water samples. The various real water samples collected are spiked with known concentrations of Hg^{2+} ions and analyzed using the DPV technique. The detection of Hg^{2+} ions in the different water samples was obtained in the range of 102–106% with an RSD in the range of 0.6–1.8% and are tabulated in Table 3. These results suggest the great potential of the AgNP-MD be used as a green synthesized sensor for Hg^{2+} ions in real water samples.

3.7 Catalytic Degradation of Organic Dyes

The catalytic activity of AgNP-MD was studied using the degradation of two organic dyes: methyl orange (MO) and methylene blue (MB). Degradation of dyes using NaBH_4 was carried out in the presence and absence of the nanocatalyst, AgNP-MD. Methyl orange is chemically sodium; 4-[[4-(dimethylamino) phenyl diazenyl benzene sulfonate, $\text{C}_{14}\text{H}_{14}\text{N}_3\text{NaO}_3\text{S}$. This azo dye is often used as an indicator in various analytical fields [42]. The aqueous solution of MO shows two absorption peaks at 464 and 264 nm. The major peak at 464 nm is due to the $-\text{N}=\text{N}-$ group. The aqueous solution of MO shows an orange-red coloration which upon complete degradation becomes completely colorless.

Methylene blue is chemically methylthioninium chloride, $\text{C}_{16}\text{H}_{18}\text{ClN}_3\text{S}$. Methylene blue is commonly used as a redox indicator in the analytical study, staining agent in biology, and for the treatment of methemoglobinemia in medicine. It is said to possess antiseptic, antimalarial, and antidepressant

properties [43]. The UV–vis spectrum shows two peaks at 290 and 664 nm with a hump at 612 nm corresponding to the $\pi \rightarrow \pi^*$ and $n \rightarrow \pi^*$ transitions, respectively. Its aqueous solution shows a deep blue color. Upon complete degradation by AgNP-MD, it forms colorless leucomethylene blue. The reduction of methyl orange and methylene blue was monitored spectrophotometrically at 464 and 664 nm in 1 min duration. The chemical structures of methyl orange and methylene blue are depicted in Fig. 17.

The degradation of the dyes in the presence of NaBH_4 alone was performed, and no color change was observed even after several hours of the reaction. Thus, dye degradation in the absence of nanocatalyst or in the presence of NaBH_4 alone is said to be negligible, due to the large difference in the redox potentials of the dye and reducing agent, NaBH_4 . Figure 18a depicts the degradation of methyl orange by 0.04 mg/mL AgNP-MD. Methyl orange on reduction shows a color change from orange-red to colorless. The degradation was completed

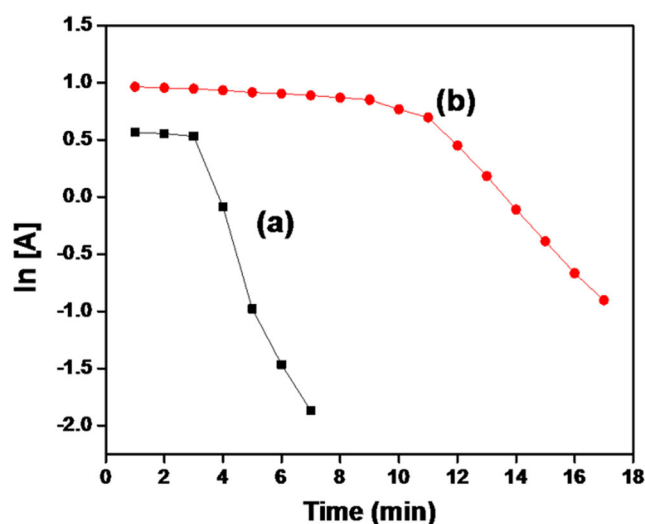


Fig. 19 Plots of $\ln [A]$ against time for the degradation of **a** methyl orange and **b** methylene blue using 0.02 mg/mL concentration of AgNP-MD catalyst

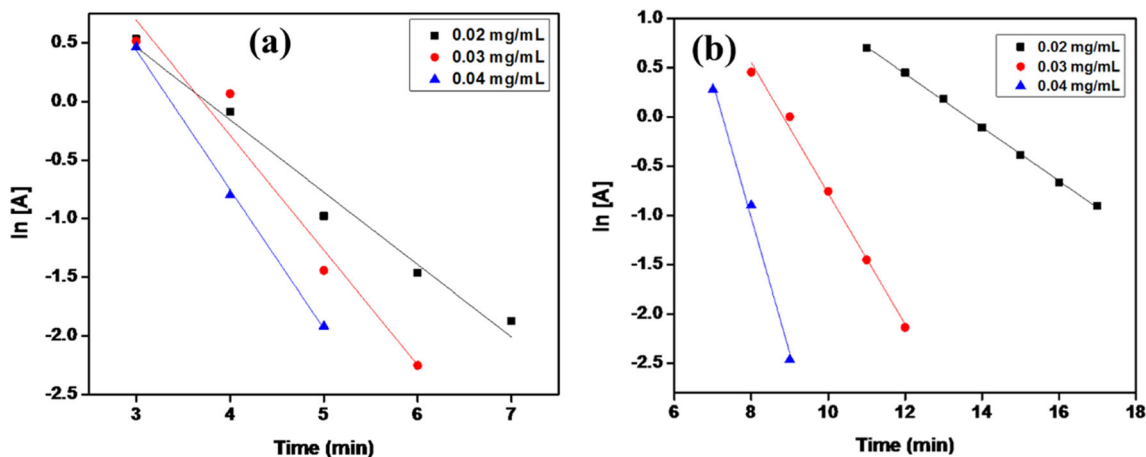


Fig. 20 Plots of ln [A] against time for the degradation of a methyl orange and b methylene blue using varying concentrations of AgNP-MD

in 5 min, and the intensity of the peak at 464 nm decreased continuously. A new peak at 250 nm originated due to the formation of the amino group. Upon the addition of 0.04 mg/mL AgNP-MD nanocatalyst, the original blue color of the methylene blue dye declined and ultimately became colorless. The degradation was complete within 9 min. The gradual decrease in the intensity of the peak at 664 nm is synchronized by the emergence of a new peak at 256 nm (Fig. 18b). The evolution of this new peak is ascribed due to the emerging leuco form of methylene blue. The hydrogen gas evolution during the progress of the reaction prevents re-oxidation of leuco methylene blue into blue-colored methylene blue by successive removal of oxygen from the reaction system [44]. The bubbling effect of hydrogen gas produced helps in the sequential removal of the reaction product from the catalyst surface and thus increasing the efficacy of the catalyst [45].

3.7.1 Mechanism of Catalytic Degradation

During the degradation process, a catalytic reaction occurs at the surface region of silver nanoparticles [46]. The phytochemicals surrounding the nanoparticles assist this process by attracting them towards the catalyst surface by electrostatic interaction. It involves the electron transfer between donor NaBH₄ and acceptor dye moiety [47]. The capping agents surrounding the AgNP assist the process by attracting the donor and acceptor moieties towards the catalyst surface by

means of electrostatic interaction. Due to the strong nucleophilic nature, the reductive potential of NaBH₄ decreases upon adsorption on the nanoparticle surface, while that of electrophilic dye molecules increases [48]. Upon simultaneous adsorption of both species on the nanosurface, potential becomes more negative for NaBH₄ and more positive for dye moieties. Thus, the presence of the nanocatalyst having a reduction potential intermediate between NaBH₄ and dye eases the electron relay process.

3.7.2 Kinetics Study

The reaction kinetics was monitored spectrophotometrically by the variation in absorbance of methylene blue and methyl orange peaks at 664 and 464 nm, respectively. Since the concentration of NaBH₄ used in the degradations was much higher than that of dyes and nanocatalyst, it remains practically constant during the course of the reaction. Hence, the degradation follows pseudo-first-order kinetics. Rate equation can be written as $k = 1/t \ln [A_0]/[A]$. k is the pseudo-first-order rate constant, $[A_0]$ is the initial concentration of the dye, and $[A]$ is the concentration at time t . Therefore, the plot of $\ln [A]$ versus time gives a straight line with rate constant as slope.

An induction period (IP) was observed at the initial stages for the degradation of both methyl orange and methylene blue dyes. The delay time observed is larger for methylene blue

Table 4 Catalytic activity of AgNP-MD in the degradation of methyl orange

Concentration of AgNP (mg mL ⁻¹)	Time (min)	Rate constant k (min ⁻¹)	Correlation coefficient (R ²)
0.02	7	0.6181	0.9740
0.03	6	0.9815	0.9437
0.04	5	1.1886	0.9977

Table 5 Catalytic activity of AgNP-MD in the degradation of methylene blue

Concentration of AgNP (mg mL ⁻¹)	Time (min)	Rate constant k (min ⁻¹)	Correlation coefficient (R ²)
0.02	17	0.2716	0.9991
0.03	12	0.6639	0.9928
0.04	9	1.3717	0.9863

Table 6 Comparison of catalytic activities of AgNP-MD with reported green synthesized silver nanoparticles

Dye	Green silver nanoparticles	Rate constant (min ⁻¹)	Reference
Methyl orange	AgNP- <i>Anacardium occidentale</i>	0.1178	[50]
	AgNP- <i>Biophytum sensitivum</i>	0.2758	[45]
	AgNP- <i>Nervalia zeylanica</i>	0.2860	[51]
	AgNP- <i>Punica granatum</i>	0.5477	[52]
	AgNP- <i>Morinda citrifolia</i>	0.6402	[53]
	AgNP- <i>Coscinium fenestratum</i>	0.8750	[44]
Methylene blue	AgNP- <i>Mimosa diplotricha</i>	1.1886	This work
	AgNP- <i>Morinda citrifolia</i>	0.0320	[53]
	AgNP- <i>Convolvulus arvensis</i>	0.1080	[54]
	AgNP- <i>Punica granatum</i>	0.1904	[52]
	AgNP- <i>Myxopyrum serratum</i>	0.6410	[33]
	AgNP- <i>Bauhinia purpurea</i>	0.8153	[55]
	AgNP- <i>Biophytum sensitivum</i>	1.3080	[45]
	AgNP- <i>Mimosa diplotricha</i>	1.3717	This work

than that of methyl orange dye. This is assigned to the hydrophobicity proposed by the presence of four methyl groups in methylene blue which hampers the proper contact of methylene blue with the AgNP-MD nanocatalyst [49]. After IP, both degradations were observed to be smooth and linear (Fig. 19). The induction time is said to be the time taken by the nucleophilic NaBH₄ moieties to expel the oxide layer formation on the catalyst surface due to their interaction with atmospheric oxygen and consequently to activate the catalyst [45]. The delay time was found to decrease with an increase in the concentration of the AgNP-MD catalyst.

To study the influence of catalyst dosage, the reactions were carried out using varying concentrations of AgNP-MD, keeping all other parameters constant (Fig. S2 and S3 of Supplementary material). All the reactions were monitored by a UV-vis spectrophotometer. The ln [A] values corresponding to the 464 and 664 nm of methyl orange and methylene blue dyes were plotted against time (Fig. 20). In both cases, the linear plot shows that the rate constant (k) increases linearly with the increase in the concentration of the catalyst. The reactions are very fast, and they all follow pseudo-first-order kinetics with good correlation coefficient values, which are clearly depicted in Tables 4 and 5. Rate constants of both the degradation reactions are higher than those of the reported ones (Table 6). Thus, the green synthesized AgNP-MD acts as an effective catalyst for the degradation of organic dyes and is a potential candidate for wastewater purification.

4 Conclusions

In the present study, microwave-assisted green synthesis of silver nanoparticles was established using *Mimosa diplotricha* leaf

extract. The phytoconstituents present in the aqueous leaf extract act as the reducing and stabilizing agent for AgNP-MD synthesis. The crystalline spherical nanoparticles showed an average particle size of 13.88 nm. The green synthesized AgNP-MD acts as a reliable optical and electrochemical sensor for the detection of Hg²⁺ ions in an aqueous solution. The LOD was calculated to be 1.46 μM from the DPV analysis. The synthesized AgNP-MD and its effective interaction with Hg²⁺ ions were characterized by UV-vis, FT-IR, XRD, TEM, and EDX techniques. The DLS and zeta potential measurements confirm the formation of AgNP-MD-Hg²⁺. The designed sensor successfully detected mercury ions in real water samples with detection of 102–106% with an RSD of 0.6–1.8%. Hence, the development of a green synthesized AgNP-MD sensor for the accurate and efficient sensing of toxic Hg²⁺ ion in aqueous solution opened a new window in the analytical and industrial applications. The AgNP-MD shows good catalytic potential in the degradation of methyl orange and methylene blue dyes. Time for degradation of dyes decreased with an increase in the concentration of the nanocatalyst. Thus, the green synthesized AgNP-MD plays a dual role as a sensor for the detection of Hg²⁺ ions and also as a coherent catalytic agent for the reduction of hazardous dye pollutants. This green approach towards nanoparticle synthesis offers several advantages and attractions including environmental protection.

Supplementary Information The online version contains supplementary material available at <https://doi.org/10.1007/s12668-021-00883-w>.

Author Contribution Mamatha Susan Punnoose: conceptualization, methodology, resources, and writing — original draft. Bijimol D.: data curation and visualization. Thomas Abraham: data curation and visualization. Neena John Plathanam: data curation and visualization. Beena Mathew: conceptualization, supervision, project administration, and writing — review and editing.

Funding Statement Mamatha Susan Punnoose is thankful to the University Grants Commission (UGC) for the financial assistance (SRF).

Data Availability All data generated or analyzed during this study are included in this manuscript and its supplementary information files.

Code Availability Not applicable.

Declarations

Consent to Participate All authors agree to participate in this investigation.

Consent for Publication All authors agree to participate in this article.

Conflict of Interest The authors declare no competing interests.

Research Involving Humans and Animals Statement The study does not involve the use of humans or animals.

References

1. Driscoll, C. T., Mason, R. P., Chan, H. M., Jacob, D. J., & Pirrone, N. (2013). *Environmental Science & Technology*, *47*, 4967.
2. Tchounwou, P. B., Ayensu, W. K., Ninashvili, N., & Sutton, D. (2003). *Environmental Toxicology*, *18*, 149.
3. Farhadi, K., Forough, M., Molaei, R., Hajizadeh, S., & Rafipour, A. (2012). *Sensors and Actuators B: Chemical*, *161*, 880.
4. Ganguly, M., Mondal, J., Pal, J., Pal, A., Negishi, Y., & Pal, T. (2014). *Dalton Transactions*, *43*, 11557.
5. Jeevika, A., & Shankaran, D. R. (2016). *Materials Research Bulletin*, *83*, 48.
6. Zhang, Y., & Adeloju, S. B. (2015). *Talanta*, *137*, 148.
7. Karunasagar, D., Arunachalam, J., & Gangadharan, S. (1998). *Journal of Analytical Atomic Spectrometry*, *13*, 679.
8. Durkalec, M., Szkoda, J., Kolacz, R., Opalinski, S., Nawrocka, A., & Zmudzki, J. (2015). *International Journal of Environmental Research*, *9*, 205.
9. Ichinoki, S., Kitahata, N., & Fujii, Y. (2004). *Journal of Liquid Chromatography and Related Technologies*, *27*, 1785.
10. Kuswandi, B., Nuriman, H. H., & Dam, D. N. (2007). Reinhoudt and W. Verboom. *Analytica Chimica Acta*, *591*, 208.
11. Sebastian, M., Aravind, A., & Mathew, B. (2018). *Nanotechnology*, *29*, 355502.
12. Cyril, N., George, J. B., Joseph, L., & Sylas, V. P. (2019). *Journal of Cluster Science*, *30*, 459.
13. George, J. M., & Mathew, B. (2019). *Materials Research Express*, *6*, 1150h5.
14. Forough, M., & Farhadi, K. (2010). *Turkish Journal of Engineering and Environmental Sciences*, *34*, 281.
15. Xue, X., Wang, F., & Liu, X. (2011). *Journal of Materials Chemistry*, *21*, 13107.
16. Sharma, K., Singh, G., Singh, G., Kumar, M., & Bhalla, V. (2015). *RSC Advances*, *5*, 25781.
17. Davarpanah, J., & Kiasat, A. R. (2013). *Catalysis Communications*, *41*, 6.
18. Jeevika, A., & Ravi Shankaran, D. (2014). *Colloids and Surfaces A: Physicochemical and Engineering Aspects*, *461*, 240.
19. Wiley, B., Sun, Y., & Xia, Y. (2007). *Accounts of Chemical Research*, *40*, 1067.
20. Sebastian, M., Aravind, A., & Mathew, B. (2019). *BioNanoScience*, *9*, 373.
21. Joseph, S., & Mathew, B. (2015). *Spectrochimica Acta A*, *136*, 1371.
22. Oliveira, L. S., Franca, A. S., Alves, T. M., & Rocha, S. D. F. (2008). *Journal of Hazardous Materials*, *155*, 507.
23. Nasrollahzadeh, M., Atarod, M., Jaleh, B., & Gandomirouzbahani, M. (2016). *Ceramics International*, *42*, 8587.
24. Glover, B., & Pierce, J. H. (1993). *Journal of the Society of Dyers and Colourists*, *109*, 5.
25. Alaton, I. A., & Balcioglu, I. A. (2001). *Journal of Photochemistry and Photobiology A*, *141*, 247.
26. Faisal, M., Abu Tariq, M., & Muneer, M. (2007). *Dyes and Pigments*, *72*, 233.
27. Bhakya, S., Muthukrishnan, S., Sukumaran, M., Muthukumar, M., Kumar, S. T., & Rao, M. V. (2015). *Journal of Bioremediation & Biodegradation*, *6*, 312.
28. Ghosh, S. K., Kundu, S., Mandal, M., & Pal, T. (2002). *Langmuir*, *18*, 8756.
29. Caudo, S., Centi, G., Genovese, C., & Perathoner, S. (2006). *Topics in Catalysis*, *40*, 207.
30. Madathil, S. M., Kannappan, P., Kanakasabapathy, D., Varghese, S., & Muneeswari, P. (2020). *International Journal of Research in Pharmaceutical Sciences*, *11*, 4378.
31. Uyi, O. O., Udeogwu, C. C., & Rotimi, J. (2020). *Journal of Applied Sciences and Environmental Management*, *24*, 645.
32. Aravind, A., Sebastian, M., & Mathew, B. (2018). *New Journal of Chemistry*, *42*, 15022.
33. Vijayan, R., Joseph, S., & Mathew, B. (2017). *BioNanoScience*, *8*, 105.
34. Park, H.-H., Zhang, X., Choi, Y.-J., Park, H.-H., & Hill, R. H. (2011). *Journal of Nanomaterials*, *2011*, 1.
35. Meléndrez, M. F., Cárdenas, G., & Arbiol, J. (2010). *Journal of Colloid and Interface Science*, *346*, 279.
36. Rex, M., Hernandez, F. E., & Campiglia, A. D. (2006). *Analytical Chemistry*, *78*, 445.
37. Manivannan, S., Seo, Y., Kang, D.-K., & Kim, K. (2018). *New Journal of Chemistry*, *42*, 20007.
38. Sowmya, T., & Lakshmi, V. G. (2017). *BioNanoScience*, *8*, 179.
39. Lobregas, M. O. S., Bantang, J. P. O., & Camacho, D. H. (2019). *Sensing and Bio-Sensing Research*, *26*, 100303.
40. Proposito, P., Burratti, L., Bellingeri, A., Protano, G., Faleri, C., Corsi, I., Battocchio, C., Iucci, G., Tortora, L., Secchi, V., Franchi, S., & Venditti, I. (2019). *Nanomaterials*, *9*, 1353.
41. Eksin, E., Erdem, A., Fafal, T., & Kivçak, B. (2019). *Electroanalysis*, *31*, 1075.
42. Mittal, A., Malviya, A., Kaur, D., Mittal, J., & Kurup, L. (2007). *Journal of Hazardous Materials*, *148*, 229.
43. Clifton, J., & Leikin, J. B. (2003). *American Journal of Therapeutics*, *10*, 289.
44. Ragam, P. N., & Mathew, B. (2019). *International journal of Environmental Science and Technology*, *17*, 1739.
45. Joseph, S., & Mathew, B. (2015). *Journal of Molecular Liquids*, *204*, 184.
46. Grogger, C., Fattakhov, S., Jouikov, V., Shulaeva, M., & Reznik, V. (2004). *Electrochimica Acta*, *49*, 3185.
47. Pal, T., De, S., Jana, N. R., Pradhan, N., Mandal, R., Pal, A., Beezer, A. E., & Mitchell, J. C. (1998). *Langmuir*, *14*, 4724.
48. Punnoose, M. S., & Mathew, B. (2018). Treatment of water effluents using silver nanoparticles. *Material Science & Engineering International Journal*, *2*, 345.
49. Azad, U. P., Ganesan, V., & Pal, M. (2011). *Journal of Nanoparticle Research*, *13*, 3951.
50. Edison, T. N. J. I., Atchudan, R., Sethuraman, M. G., & Lee, Y. R. (2016). *Journal of Photochemistry and Photobiology. B*, *162*, 604.

51. Vijayan, R., Joseph, S., & Mathew, B. (2018). *Particulate Science and Technology*, **37**, 809.
52. Kumari, M. M., & Philip, D. (2015). *Spectrochimica Acta. Part A, Molecular and Biomolecular Spectroscopy*, **135**, 632.
53. Francis, S., Nair, K. M., Paul, N., Koshy, E. P., & Mathew, B. (2019). *Materials Today: Proceedings*, **9**, 97.
54. Hamed, S., Shojaosadati, S. A., & Mohammadi, A. (2017). *Journal of Photochemistry and Photobiology. B*, **167**, 36.
55. Vijayan, R., Joseph, S., & Mathew, B. (2018). *Bioprocess and Biosystems Engineering*, **42**, 305.

Publisher's Note Springer Nature remains neutral with regard to jurisdictional claims in published maps and institutional affiliations.